Theory of Intersubband Raman Laser in Modulation-doped Asymmetric Coupled Double Quantum Wells

S. M. Maung and S. Katayama

School of Materials Science, Japan Advanced Institute of Science and Technology,

1-1 Asahidai, Tatsunokuchi, Ishikawa 923-1292

(Received May 31, 2004)

ABSTRACT

A microscopic theory is developed for the laser gain due to stimulated intersubband electronic Raman scattering pumped by CO_2 laser in modulation-doped GaAs/AlGaAs asymmetric coupled double quantum wells (ACDQWs). Based on the charge-density-excitation (CDE) mechanism, the formula for electronic Raman scattering cross-section is given, taking into account the coupling between intersubband plasmon and optical phonons including GaAs confined LO phonons and interface phonons. Stimulated Raman gain factor is then derived from the cross-section. The optimization of Raman gain, the gain saturation and threshold condition are also discussed. Numerical analysis for temporal variation of stimulated Stokes photon density, subband populations and output Raman laser power is carried out by using the self-consistent conventional rate equations. The theory can predict the presence or lack of coupled modes in lasing in well consistent with the recent experimental results.

KEYWORDS: intersubband Raman laser, electron-phonon interaction, modulation-doped asymmetric quantum wells

1. Introduction

Finding the new sources for mid- and far-infrared semiconductor lasers (wavelength 1~20 μm) has attracted much attention of researchers because of increasing requirements for trace gas analysis, remote chemical sensing, laser radar and wide-band communications etc. As the most attractive source, development of electrically pumped unipolar semiconductor quantum cascade (QC) laser has proved its importance in physics and device applications.[1,2] However, in optimizing the population inversion and electron transport in cascading through the active regions, it must rely on the complicated design of the state-of-the art epitaxy method. In adddition, the presence of doped injectors and contact layers makes long-wavelength radiation difficult to achieve because free-carrier absorption-losses dramatically increase above 11 μm.[3] Therefore, the second development of the alternate type of unipolar laser based on conduction-intersubband transitions, the so-called quantum fountain (QF) laser, was realized in GaAs/AlGaAs coupled quantum wells.[4,5] Unlike the QC lasers, QF lasers use the optical pumping by CO_2 laser. Population inversion between the upper and lower laser levels is achieved by the fast electron relaxation from the lower laser level into the ground subband level mediated by LO phonon scattering. With no current flow and not necessary of doped cladding layers and metal contacts, there are low internal losses at long wavelengths due to free carrier absorption. QF lasers were then expected to have better performance in output power than QC lasers at longer wavelengths above 10 μm. However, there is a difficulty in gain optimization by independent control of the quantum well and barrier widths, because it requires both the large stimulated emission cross-section and population inversion between the subbands.[6]

More recently, making use of the stimulated Raman effect, unipolar three-level conduction-intersubband Raman laser (IRL) pumped by CO_2 laser has been proposed[6] and also been realized experimentally[7,8] for mid-infrared radiation (10~15 μm) in modulation-doped GaAs/AlGaAs asymmetric coupled double quantum wells (ACDQWs) system. In contrast to QF laser, the use of

Raman process in IRL has the advantage of providing independent control for emission cross-section and effective lasing life-time to get the optimal Raman gain. In the early stage of the development of IRLs, only one kind of AlAs-like optical phonon mode was observed in the Stokes Raman process in the ACDQWs structure that was used [7], and from the analysis of electron-phonon coupling matrix element this is expected to be a AlAs-like interface (IF) mode coming from the barriers of the ACDQWs structure.[8] Interestingly, later experiments with use of several ACDQWs samples have revealed a new picture of the coupled-mode behavior in Raman lasing between the bulk phonons and the intersubband plasmon, and by using a simple phenomenological coupled mode solution these phonons are assumed to be the GaAs and AlGaAs-like bulk LO phonons.[9] However, the reasons for the selective presence or lack of coupled modes containing also coupling with IF phonon modes observed in lasing processes in all the above experiments have not been explained yet. Moreover, the microscopic origin of these coupled modes and their role of importance have not been fully understood. In a theoretical treatment of IRL, Khurgin *et al.* in ref. 6 derived the Raman gain from the third-order nonlinear susceptibility tensor $\chi^{(3)}$ deduced from the coupling of the electromagnetic waves[10], and pointed out the advantages of use of the Raman effect in lasing compared to QF lasers. However, their approach can not be readily applied to the present ACDQWs-based IRL devices, because the lasing in IRL is mediated by the coupled electron-phonon modes, not by the pure phonon modes with known frequencies. In particular, their nonlinear susceptibility tensor can not reveal the microscopic origins of these coupled modes in lasing process, and will not be able to predict the lasing Stokes frequencies found in the experiments.[7–9] Therefore it still remains to develop a microscopic theory of intersubband Raman lasing process in the presence of coupled electron-phonon modes under the presence of intense optical pumping laser and Stokes fields.

In the present paper we give a theory of optically pumped unipolar intersubband Raman laser realized in modulation-doped GaAs/AlGaAs ACDQWs. We explore a new theoretical

approach for the derivation of Raman gain in ACDQWs based on the stimulated electronic Raman scattering due to charge-density-excitation (CDE) mechanism. The theory can predict the lasing frequencies shifted from CO_2 pumping frequencies by the amount of the frequency of one of the coupled intersubband plasmon-phonon modes in which both the confined LO phonons and IF optical phonons are considered for coupling with intersubband plasmon. This is well consistent with the experimental results.[9] In addition, we find that the electron-optical phonon coupling strengths are determined by the electrostatic potential profiles of phonon modes, and these in turns strongly depend on the structural parameters of ACDQWs. These coupling strengths determine the frequencies and relative magnitude of intensities of the coupled modes observed in stimulated Raman scattering.

The content of this paper is as follows. In §2, we discuss the electron-phonon interaction in ACDQWs. Two kinds of optical phonons: confined LO phonons and the interface (IF) optical phonons, can couple with the electrons in ACDQWs. We first explore the dispersion relation and electrostatic potential of each phonon, and then electron-phonon interaction Hamiltonian is given. Section 3 is devoted to the derivation of Raman scattering cross-section due to the charge-density-excitation in conduction subbands, taking into account the many-body electron-electron and electron-optical phonon interactions. The density-density correlation function that appears in the cross-section is then related to the electron Green's function within the random phase approximation (RPA) framework.[11] We find the coupled intersubband plasmon-phonon collective excitation from the Dyson equation of the dynamical response function χ and give the final form of spectral differential scattering cross-section in ACDQWs. The stimulated Raman gain factor is derived from the scattering cross-section and the self-consistent rate equations for the population dynamics in subbands are developed. The way for optimization of Raman gain is then given. The saturated gain at high-intensity pumping levels and the threshold gain is also derived. We adopt our theory in §4

to analyze the GaAs/AlGaAs ACDQWs structures, and the calculated results are discussed in comparison with the recent experimental results. Finally, concluding remarks are given in §5.

2. Electron-optical phonon interactions in ACDQWs

The ACDQWs structure consists of periodic multiple quantum wells (MQW) with each period containing two coupled wells (widths w_1 and w_2), a very thin central barrier (width b_2) and the two wider outside barriers (widths $b_1/2$) which are n-type modulation-doped at their centers, as displayed schematically in Fig. 1. The well and barrier layers are made by the binary (GaAs) and ternary ($Al_xGa_{1-x}As$) mixed materials, respectively. Each well is populated by two dimensional electron gas (2DEG), and consequently the band bending and self-consistent electronic subband structures are formed in ACDQWs. These 2D electrons are coupled with the optical phonon modes of ACDQWs.

The two kinds of optical phonons, confined LO phonon and interface (IF) phonon, are to be considered for the electron-phonon interactions in ACDQWs. The dielectric functions of binary and ternary mixed materials making the wells and barrier layers in ACDQWs, respectively, can be described as

$$\varepsilon_w(\omega) = \varepsilon_{\infty w}\frac{(\omega^2-\omega_{Lw}^2)}{(\omega^2-\omega_{Tw}^2)},$$

and

$$\varepsilon_b(\omega) = \varepsilon_{\infty b}\frac{(\omega^2-\omega_{Lb1}^2)(\omega^2-\omega_{Lb2}^2)}{(\omega^2-\omega_{Tb1}^2)(\omega^2-\omega_{Tb2}^2)}, \tag{1}$$

where the suffix $w(b)$ corresponds to well(barrier) and suffix 1(2) denotes two kinds of LO phonons in ternary mixed material, e.g. GaAs-like and AlGaAs-like phonons in $Al_xGa_{1-x}As$ layer, and ε_∞ is the high frequency dielectric constant in each layer. Following the dielectric continuum approach[12-15], the basic electrostatic equation that the phonon modes satisfy in each layer is

$$\varepsilon_i(\omega)\left(\frac{\partial^2}{\partial z^2}-q^2\right)\psi^{\mathrm{ph}}(q,z)=0, \tag{2}$$

where suffix $i = w(b)$, $\psi^{\mathrm{ph}}(q,z)$ is two-dimensional (2D) Fourier transform of scalar potential of each phonon mode in the q-z plane, k being the magnitude of 2D wave vector $\mathbf{q}=(q_x,q_y)$. Taking the boundary conditions that $\psi^{\mathrm{ph}}(q,z)$ and $\varepsilon_i(\partial\psi^{\mathrm{ph}}/\partial z)$ are continuous across the interfaces, the phonon frequencies and dispersion relations can be determined by eq. (2). The condition of $\varepsilon_i(\omega)=0$ yields the dispersionless confined LO phonon modes with the same frequency as that of bulk LO phonon. We have derived the normalized electrostatic coupling-potential energy defined by $\phi^{\mathrm{ph}}(q,z)=e\psi^{\mathrm{ph}}(q,z)$ with electronic charge e. Therefore for the confined-LO phonon modes we have

$$\phi^{\mathrm{ph}}_{j,m}(q,z)=\left\{\begin{array}{ll}\left\{\dfrac{4\pi e^2\hbar\omega_{\mathrm{LO}}}{A}\left(\dfrac{1}{\varepsilon_\infty}-\dfrac{1}{\varepsilon_0}\right)\right\}^{1/2}\left(\dfrac{1}{w_j\{q^2+(\dfrac{m\pi^2}{w_j})^2\}}\right)^{1/2}\sin\left(\dfrac{m\pi z-\frac{w_j}{2}}{w_j}\right) & \\ \qquad\qquad\qquad\qquad\qquad\qquad\qquad\qquad\qquad\qquad \text{when } -\dfrac{w_j}{2}<z<\dfrac{w_j}{2}, & \\ =0 \qquad\qquad\qquad\qquad\qquad\qquad\qquad\qquad\qquad\qquad \text{otherwise,} & \end{array}\right. \tag{3}$$

where A is the in-plane area, j =1,2 corresponds to well 1 or 2 and the quantum number m takes the positive integer values.

For the case of $\varepsilon_i(\omega)\neq 0$, solutions of eq. (2) using the boundary conditions give the frequencies and dispersion relations of IF modes in ACDQWs. The electrostatic potential energy $\Phi_i(\mathbf{r})$ of IF phonons in each layer of ACDQWs is given by its 2D Fourier transform $\phi^{\mathrm{ph}}(q,z)$ as

$$\Phi(\mathbf{r}) = \sum_{\mathbf{q},l} e^{i\mathbf{q}\cdot\mathbf{r}} \phi_l^{\mathrm{ph}}(q,z). \tag{4}$$

where $\mathbf{r} = \{\rho, z\}$, $\rho = \{x, y\}$ and the suffix l counts all IF modes found in ACDQWs.

We apply the effective transfer matrix method[16] to determine the dispersion relations and electrostatic potentials of IF modes, and found 12 IF modes in total in our ACDQWs since there are 4 interfaces in each period. The calculated dispersion relations and electrostatic potentials of 6 IF modes out of 12, for small 2D wave vectors involved in the Raman scattering will be shown in 3. There are symmetric and antisymmetric modes for each group of IF phonon modes, i.e. AlAs-like, GaAs and GaAs-like modes.

Then the quantum mechanical Hamiltonian of single electron-optical phonon interaction can be described in terms of the potential energies of each phonon mode in the form of

$$H_{\text{e-ph}} = \sum_{\mathbf{q},\nu} e^{i\mathbf{q}\cdot\boldsymbol{\rho}} \phi_\nu^{\mathrm{ph}}(q,z)\ (b_{-\mathbf{q},\nu}^{+} + b_{\mathbf{q},\nu}), \tag{5}$$

where $\nu = \{m,l\}$. The functional forms of $\phi_\nu^{\mathrm{ph}}(q,z)$ are given by eqs. (3) and (4) for confined LO phonon and IF phonon, respectively, and b, b^{+} are the destruction and creation operators for each phonon mode.

3. Microscopic Theory for stimulated Raman lasing in ACDQWs

In practical IRL devices, the side pumping and laser emission along the direction of facets in ACDQWs has been utilized in experiments [9] as depicted in Fig. 2 (a). With optical pumping by an intense laser field from an initial subband state $\tilde{n}$ to a virtual state n close to a real subband state, stimulated Stokes lasing occurs between that virtual state and the final subband state $\tilde{n}'$ in ACDQWs as illustrated in Fig. 2 (b). In order to develop a microscopic theory for the stimulated Raman lasing process, we consider the 2DEG with electron-electron and electron-phonon interactions in the total Hamiltonian of

$$H = H_{\mathrm{e}} + H_{\mathrm{e\text{-}e}} + H_{\mathrm{ph}} + H_{\mathrm{e\text{-}ph}}. \tag{6}$$

Each term represents as

$$H_{\mathrm{e}} = \sum_{\mathbf{k}n} E_n(\mathbf{k}) C^{+}_{\mathbf{k},n} C_{\mathbf{k},n},$$

$$H_{\mathrm{e\text{-}e}} = \frac{1}{2} \sum_{\mathbf{kpq}} \sum_{nn'\tilde{n}\tilde{n}'} V_q^{\mathrm{Coul}} C^{+}_{\mathbf{k}+\mathbf{q},\tilde{n}} C^{+}_{\mathbf{p}-\mathbf{q},n'} C_{\mathbf{p},n} C_{\mathbf{k},\tilde{n}} \int dz \int dz' \zeta_{\tilde{n}'}(z') \zeta_{n'}(z) \zeta_n(z) \zeta_{\tilde{n}}(z') e^{-iq|z-z'|},$$

$$H_{\mathrm{ph}} = \sum_{\mathbf{q},\nu} \frac{1}{2} \left(P^{+}_{\mathbf{q},\nu} P_{\mathbf{q},\nu} + \omega^2_{\mathbf{q},\nu} Q^{+}_{\mathbf{q},\nu} Q_{\mathbf{q},\nu} \right),$$

$$H_{\mathrm{e\text{-}ph}} = \sum_{\mathbf{pq}} \sum_{nn'} \sum_{\nu} C^{+}_{\mathbf{p}+\mathbf{q},n'} C_{\mathbf{p},n} (b^{+}_{-\mathbf{q},\nu} + b_{\mathbf{q},\nu}) \int dz\, \zeta_{n'}(z) \zeta_n(z)\ \phi^{\mathrm{ph}}_{\nu}(\mathbf{q},z),$$

where $E_n(\mathbf{k}) = E_n + \hbar^2 k^2 / 2m^*$ and $\zeta_n(z)$ are the subband energy and corresponding envelope functions, and C, C^{+} are the electron creation and destruction operators. The vectors **k**, **p**, **q** denote 2D in-plane wave vectors, $nn'\tilde{n}\tilde{n}'$ are subband indices. $P_{\mathbf{q},\nu}$ and $Q_{\mathbf{q},\nu}$ are the canonical momentum and coordinates of the phonon's normal modes. $V_q^{\mathrm{Coul}} = (2\pi e^2 / A\, q\varepsilon_{\infty})$ is the Fourier components of 2D electron-electron Coulomb interaction. We do not show explicitly the spin indices in the above Hamiltonians because the spin states are not changed in the CDE Raman scattering process.

3.1 Derivation of intersubband Raman Scattering Cross-section

In the second quantized formalism radiation states are quantized through use of the vector potential **A** and the electron-radiation field interaction Hamiltonian is written as

$$H_{\mathrm{e\text{-}rad}} = \int d\mathbf{r}\, \Psi^{+}(\mathbf{r}) \left(\frac{e}{m^* c} \right) \mathbf{p} \cdot \mathbf{A}(\mathbf{r}) \Psi(\mathbf{r}), \tag{7}$$

where the electron field operators are $\Psi(\mathbf{r}) = \sum_{\mathbf{k},n} C_{\mathbf{k},n} |n;\mathbf{k}\rangle$, and the state $|n;\mathbf{k}\rangle$ consists of subband envelope function $F_{n,\mathbf{k}}(r) = (L_x L_y)^{1/2} e^{i\mathbf{k}\cdot\boldsymbol{\rho}} \zeta_n(z)$ and the conduction band lattice periodic function $U_c(\mathbf{r})$. For a two-photon Raman scattering process as shown in Fig. 2 (b), transition probability W

from the many-body initial state I to the final state F can be described by the second-order matrix element T using the Fermi-golden rule

$$W_{FI} = (2\pi/\hbar)\sum_{F}|T|^2\delta(E_F - E_I), \tag{8}$$

where the transition matrix element T has been derived in terms of the Raman tensor R for intersubband transitions as

$$T = \frac{2\pi\hbar e^2 n_{\mathrm{i}}^{1/2}}{m^* V(\omega_{\mathrm{s}}\omega_{\mathrm{i}})^{1/2}} \sum_{\tilde{n}\tilde{n}'}\sum_{\mathbf{k}} R_{\mathbf{k}}(\tilde{n}';\tilde{n}) \left\langle F \left| C^{+}_{\mathbf{k}+\mathbf{q},\tilde{n}'} C_{\mathbf{k},\tilde{n}} \right| I \right\rangle. \tag{9}$$

Here n_{i} is the density of incident photons and R is defined by

$$R_{\mathbf{k}}(\tilde{n}';\tilde{n}) \equiv \frac{1}{m^*}\sum_{n}\left\{ \frac{\langle \tilde{n}';k|\hat{e}_{\mathrm{s}}\cdot\mathbf{p}|n;k\rangle\langle n;k|\hat{e}_{\mathrm{i}}\cdot\mathbf{p}|\tilde{n};k\rangle}{E_{\tilde{n}}(\mathbf{k}+\mathbf{q}) + \hbar\omega_{\mathrm{i}} - E_n(\mathbf{k})} + \frac{\langle \tilde{n}';k|\hat{e}_{\mathrm{i}}\cdot\mathbf{p}|n;k\rangle\langle n;k|\hat{e}_{\mathrm{s}}\cdot\mathbf{p}|\tilde{n};k\rangle}{E_{\tilde{n}}(\mathbf{k}+\mathbf{q}) - \hbar\omega_{\mathrm{s}} - E_n(\mathbf{k})} \right\}. \tag{10}$$

Assuming the small wave vector transfer between incident and scattered light as $\mathbf{q} << \mathbf{k},\mathbf{k}'$, $R_{\mathbf{k}}$ becomes independent of $\mathbf{k}$ since $k \approx k'$. Therefore we will write $R_{\mathbf{k}} = R$ in later expressions. The spectral differential scattering cross-section due to intersubband electronic charge-density-excitation is then obtained in the form of

$$\frac{\mathrm{d}^2\sigma}{\mathrm{d}\omega\, d\Omega} = \frac{r_0^2}{2\pi}\left(\frac{\omega_{\mathrm{s}}}{\omega_{\mathrm{i}}}\right) \sum_{n\tilde{n}'nn'}\sum R^*(\tilde{n}',\tilde{n})R(n,n') \int_{-\infty}^{\infty}\mathrm{d}t\, e^{-i\omega t}\left\langle \rho_{\tilde{n}\tilde{n}'}(\mathbf{q};t)\rho^{+}_{nn'}(\mathbf{q};0)\right\rangle, \tag{11}$$

where $r_0 = e^2/(m^*c^2)$ is the classical radius of an electron having effective mass m^*. Therefore cross-section is related to the density-density correlation function defined by the charge-density excitation operator in the subbands as $\rho^{+}_{nn'}(\mathbf{q};t) = \sum_{\mathbf{k}} C^{+}_{n,\mathbf{k}+\mathbf{q}}(t)\, C_{n',\mathbf{k}}(t)$. In order to derive the correlation function, we define the Green's functions of electron-phonon coupled system in ACDQWs as follows:

$$G_{\mathrm{e\text{-}e}}(\mathbf{q};t) = -i\frac{\theta(t)}{\hbar}\left\langle [\rho_{\tilde{n}\tilde{n}'}(\mathbf{q};t), \rho^{+}_{nn'}(\mathbf{q};0)] \right\rangle, \tag{12a}$$

$$D_{\nu\text{-}\mathrm{e}}(\mathbf{q};t) = -i\frac{\theta(t)}{\hbar}\left\langle [Q_{\mathbf{q},\nu}(t), \rho_{nn'}(\mathbf{q};0)]\right\rangle. \tag{12b}$$

Finding the time-evolution of the Green's function $G_{e\text{-}e}$ in the total Hamiltonian given by eq. (6), we have derived the integral form of Dyson's equation for the dynamical response function χ of the electron-phonon coupled system[17]. Finally, the resulting matrix form of response function χ is obtained as

$$\vec{\chi}(q,\omega) = \left\{\vec{1} - \vec{V}^{\text{eff}}(q,\omega)\vec{\chi}^{0}(\omega)\right\}^{-1} \chi^{0}(\omega), \tag{13}$$

where the explicit form of $(\tilde{n}'n', n\tilde{n})$ component of $\vec{V}^{\text{eff}}(q,\omega)$ is given by

$$V^{\text{eff}}_{\tilde{n}'n',n\tilde{n}}(q,\omega) = \int dz_1 \int dz_2\, \zeta_{\tilde{n}'}(z_1)\zeta_{n'}(z_1)\left\{V_q^{\text{Coul}} e^{-q|z_1-z_2|} + \sum_{\nu} \frac{2\hbar\omega_{q,\nu}}{\hbar^2(\omega^2-\omega_{q,\nu}^2)}\phi_{\nu}^{\text{ph}*}(q,z_1)\phi_{\nu}^{\text{ph}}(q,z_2)\right\} \times \zeta_n(z_2)\zeta_{\tilde{n}}(z_2). \tag{14}$$

Here $V^{\text{eff}}_{\tilde{n}'n',n\tilde{n}}(q,\omega)$ is the effective particle-particle interaction in electron-phonon coupled system. When we limit the lowest order intersubband transition (ground subband to the first excited subband), i.e. $(\tilde{n}'n', n\tilde{n}) = (12,21) \equiv (1,1)$, eq. (13) can be solved approximately

$$\chi_{11}(q,\omega) = \frac{\chi^{0}(\omega)}{1 - V_{11}^{\text{eff}}(q,\omega)\chi^{0}(\omega)}, \tag{15}$$

in which

$$V_{11}^{\text{eff}}(q,\omega) = V_{11}^{\text{Coul}} + V_{11}^{\text{e-ph}}. \tag{16}$$

In the above equation, we have defined the strength of Coulomb interaction as

$$V_{11}^{\text{Coul}} = \frac{4\pi e^2}{\varepsilon_{\infty}} L_{11}, \tag{17}$$

with

$$L_{11} = \int \left[\int_0^z dz_1\, \zeta_1(z)\zeta_2(z_1)\right]\left[\int_0^z dz_1\, \zeta_2(z)\zeta_1(z_1)\right] dz, \tag{18}$$

L_{11} being the matrix element of Coulomb interaction in dimension of the length, and

$$V_{11}^{\text{e-ph}} = \sum_{\nu} \frac{2\hbar\omega_{q,\nu}}{\hbar^2(\omega^2 - \omega_{q,\nu}^2)} \int dz_1 \int dz_2 \zeta_1(z_1)\zeta_2(z_1)\phi_{\nu}^{\text{ph}*}(q,z_1)\phi_{\nu}^{\text{ph}}(q,z_2)\zeta_2(z_2)\zeta_1(z_2). \quad (19)$$

Therefore relating the charge density-density correlation function with the imaginary part of dynamical response function χ, spectral differential scattering cross-section of eq. (11) can then be expressed as

$$\frac{d^2\sigma}{d\omega\, d\Omega} = -\frac{r_0^2\hbar}{\pi}\left(\frac{\omega_s}{\omega_i}\right) R^*(1,2)\, R(1,2)\, [n(\omega)+1]\, \text{Im}\chi_{11}(q,\omega). \quad (20)$$

where $n(\omega)$ is the Bose-Einstein thermal distribution factor for photons. Equation (20) is the desired form for the light scattering cross-section due to coupled intersubband plasmon-phonon collective excitations in ACDQWs, which is of great importance in determining the stimulated Raman gain factor that will be considered in the following.

3.2 Stimulated Raman Gain Factor and Self-consistent Rate Equations

The transition probability W_{FI} in eq. (8) is for the spontaneous Raman scattering process in which W_{FI} is proportional to the density of incident laser photons n_i. However, if we consider the stimulated Raman process, this will be proportional to n_i (n_s +1), where n_s is the density of scattered Stokes photons. Therefore we can derive the stimulated Raman gain factor G_R from the spontaneous scattering cross-section following Bloembergen and Shen.[18] Since the change of Stokes photons N_{St}, in one mode per unit length of propagation can then be described as

$$\frac{dN_{St}}{dz} \cong (G_R - \alpha_s) N_{St}, \quad (21)$$

$$\text{where} \quad G_R = \frac{4\pi^3 c^2}{\omega_i \omega_s \varepsilon_s}(N_1 - N_2)\left\{\frac{d^2\sigma}{d(\hbar\omega)d\Omega}\right\} I_{\text{pump}}, \quad (22)$$

with the pump intensity $I_{\text{pump}} = \frac{n_i \hbar \omega_i c}{V \eta_i}$. Here V is the active volume of Raman scattering, η_i the refractive index at the incident laser frequency, N_1 and N_2 the electron populations in subbands 1 and 2, and α_s the absorption cross-section at the scattered frequency.

Equation (22) implies that IRL does not operate in the inverted population scheme. For the time dependent populations of subband 1 and 2, and number of Stokes photons, self-consistent rate equations have been derived as

$$\frac{dN_1}{dt} = -K' \frac{d^2\sigma}{d\omega_s d\Omega}(N_1 - N_2) n_i N_{St} + \frac{N_2}{\tau_{12}} - \frac{N_1}{\tau_1^{\text{eff}}}, \tag{23a}$$

$$\frac{dN_2}{dt} = K' \frac{d^2\sigma}{d\omega_s d\Omega}(N_1 - N_2) n_i N_{St} + \frac{N_1}{\tau_{21}} - \frac{N_2}{\tau_2^{\text{eff}}}, \tag{23b}$$

$$\frac{dN_{St}}{dt} = K'' \frac{d^2\sigma}{d\omega_s d\Omega}(N_1 - N_2) I_{\text{pump}} N_{St} - \frac{N_{St}}{\tau_c}, \tag{23c}$$

where $K' = (8\pi^3 c^4 / \omega_s^2 \eta_s^3)$ and $K'' = (4\pi^3 c^3 / \omega_s^2 \hbar \omega_i \eta_s^3)$. In eqs. (23a)–(23c), the relaxation times of electrons between the subbands are denoted as τ_{12} (from 2 to 1), τ_{21} (from 1 to 2), τ_1^{eff} (effective relaxation time out of 1), τ_2^{eff} (effective relaxation time out of 2) and τ_c (cavity life-time of Stokes photon).

3.3 Optimization of Raman Gain, saturated and Threshold Gain

With introducing the detuning factor δ in the Raman process such that $E_3 - E_1 + i\Gamma = \hbar\omega_i + \delta$, and considering the incoming resonance the Raman tensor in eq. (10) can be simplified as

$$R = -m^*(\omega_{23}\omega_{31} Z_{32} Z_{31}) \left\{ \frac{1}{-\delta + i\Gamma} \right\}, \tag{24}$$

where $\omega_{23}(\omega_{31})$ is the transition frequency, $Z_{32} = \int dz\zeta_3(z)z\zeta_2(z)$ or (Z_{31}) is the dipole matrix element and Γ is the linewidth of intersubband transition. Then the expression for G_R in eq. (22) can be rewritten as

$$G_R = C_1 Z_{32}^2 Z_{31}^2 \left[\frac{\hbar\Gamma}{(\delta^2+\Gamma^2)}\right] I_{pump}(N_1 - N_2), \tag{25}$$

with constant C_1 defined by

$$C_1 = -\frac{4\pi^3 c^2}{\omega_s^2 \hbar\omega_i \eta_s^2 \Gamma}\left(\frac{r_0^2}{\pi}\right)\left(\frac{\omega_s}{\omega_i}\right)(m^*\omega_{32}\omega_{31})^2[1+n(\omega)]\ \mathrm{Im}\,\chi^{11}(q,\omega). \tag{26}$$

In addition to the stimulated Raman process, we must take into account the liner absorption of subband 1 for the pump laser field via the 1→3 and 3→2 transitions, as

$$\alpha_{12} = C_2 Z_{32}^2 Z_{31}^2 \left[\frac{\Gamma^4 \tau_2^*}{(\delta^2+\Gamma^2)^2}\right] I_{pump}\, N_1, \tag{27}$$

where $\tau_2^* = \tau_2\tau_3/\tau_{32}$ is the effective lifetime of subband 2, and constant C_2 is defined by

$$C_2 = \left(\frac{4\pi\alpha_0}{\eta_i}\right)^2 \frac{\hbar\omega_s}{\Gamma^2}, \tag{28}$$

where α_0 is the fine structure constant. Therefore the net Raman Gain is given, assuming $N_1 >> N_2$, by

$$G_R^{net} = I_{pump}\, Z_{32}^2 Z_{31}^2 \left[\frac{C_1\hbar\Gamma}{(\delta^2+\Gamma^2)} - \frac{C_2\Gamma^4\tau_2^*}{(\delta^2+\Gamma^2)^2}\right] N_1. \tag{29}$$

This equation suggests that we can optimize the Raman gain by adjusting δ for a given value of Γ. The optimal detuning factor δ_{opt} has been derived as

$$\delta_{opt} = \Gamma\sqrt{\left(2\frac{C_1}{C_2}\tau_2^*\frac{\Gamma}{\hbar}\right) - 1}. \tag{30}$$

This form is similar to the one obtained in ref. 6, but our derivation for δ_{opt} contains an additional important factor (C_1/C_2) in the square root term. By using eq. (30) the optimal Raman gain is now given by

$$G_R^{net,opt} = I_{pump}\, Z_{32}^2 Z_{31}^2 \left[\frac{C_1 \hbar \Gamma}{(\delta_{opt}^2 + \Gamma^2)} - \frac{C_2 \Gamma^4 \tau_2^*}{(\delta_{opt}^2 + \Gamma^2)^2} \right] N_1. \tag{31}$$

From the spatial growth rate of Stokes laser photons as given by eq. (21), we can now determine the threshold Raman gain for one round trip in the laser cavity having length L_c, reflectivity R_1 and R_2 in the two facets, as

$$G_R^{th} = \frac{1}{2L_c} \left(\ln \frac{1}{R_1 R_2} \right) + \alpha_s. \tag{32}$$

Therefore the threshold pump intensity I_{th} can also be determined by equating eqs. (31) and (32).

At high-intensity pumping levels, population of subband 2 (N_2) will significantly increase, and thus we can no longer take $N_1 >> N_2$ in arriving at eq. (29). If we take account of this fact, it will give rise to the reduction of the Raman gain in eq. (31). The saturated Raman gain G_{sa} can then be derived as[19]

$$G_{sat} = \frac{G_R^{net,opt}}{\left\{ 1 + \dfrac{I_{pump}}{I_{sat}} \right\}}, \tag{33}$$

where the saturated intensity I_{sat} possessed by the gain medium is

$$I_{sat} = \frac{\hbar \omega_i}{2 \sigma \tau_2^*}, \tag{34}$$

with the absorption cross-section $\sigma = \alpha_{12} / N_1$.

4. Numerical Calculations and Discussion

We considered GaAs/$Al_{0.35}Ga_{0.65}As$ ACDQWs samples with different structural parameters. For optical resonant pumping by tunable CO_2 laser (wavelength 9.6~10.6 μm) from subband 1 to a virtual state close to subband 3 and Stokes scattering from that state to subband 2, appropriate subband structures must be used. We have carried out the self-consistent subband structure calculations with varying well widths. In these calculations, we take the well widths of ACDQWs such that w_1=70~80 Å, w_2=45~60 Å, and b_1 and b_2 are fixed at 200 and 11.3 Å, respectively, at doping concentration $N_{DOP} = 2.14\times10^{17}$ cm^{-3}. In Fig. 3 the self-consistent conduction band profile and the electron wave functions of three subbands are shown for a structural parameters; w_1=75 Å, w_2=60 Å, 2D sheet density $N_s = 3\times10^{11}$ cm^{-2} at T=80 K. As shown in the figure subband level separation E_3-E_1 is to be adjusted for CO_2 laser pumping and the separation E_2-E_1 is designed to be close to one of the optical phonon-mode frequencies in ACDQWs.

We have calculated the spectral differential scattering cross-section by using eq. (18). Raman tensor R can be estimated numerically by eq. (10) using the calculated subband energies and wave functions. In the calculation of imaginary part of χ, an important part is played by the effective interaction V_{11}^{eff} of electron-phonon coupled system, including the electron-electron Coulomb interaction and electron-optical phonons (confined LO and IF phonons) interaction as described by eq. (14). While assuming the confined LO phonon to be dispersionless, the frequencies of IF phonon depend on the 2D in-plane wave vector q. In Fig. 4 we plot the dispersion relations of IF phonon modes in a sample ACDQWs with w_1=75 Å, w_2=60 Å. In the figure we can notice that for small wave vector transfer involved in Raman scattering process, only 6 IF phonon modes would be observed. As indicated in Fig. 5 (a), we calculated the normalized electrostatic potentials of IF phonon modes in a ACDQWs sample with given structural parameters by assuming qb_1~0.016. The appearing 6 IF phonon modes (symmetric and antisymmetric) are named as AlAs-

like 1 and 2, GaAs 1 and 2, and GaAs-like 1 and 2. For other two samples with (b) w_1=76 Å, w_2=53 Å and (c) w_1=78 Å, w_2=50 Å are shown in Figs. 5 (b) and (c). We find that the electrostatic potentials depend strongly on the structural parameters of ACDQWs, and these will in turn lead to the different coupling strengths of electron-phonon interaction.

We will demonstrate the importance of electron-phonon coupling strength in determining the scattering cross-section. To show it, we first calculate the scattering cross-section for a sample ACDQWs with the same structural parameters as those in Fig. 4, but assuming that all the electron-phonon coupling strengths are the same as that for the confined LO phonon. Figure 6 shows the calculated spectral differential scattering cross-section versus Raman shift. We can see the coupling behavior of optical phonon modes (confined LO phonon and IF phonons) with electrons, showing the clear peaks shifted around the corresponding frequencies. The largest peak near 25 meV comes from the lower branch of coupled intersubband plasmon-GaAs confined LO phonon mode (I^-), and also the upper branch mode (I^+) and other modes coupled with IF phonons can be seen clearly.

Next, by using the actual electrostatic potentials for all phonon modes and the electron wave functions in the electron-phonon effective interaction $V_{11}^{e\text{-}ph}$, the spectral differential scattering cross-sections were calculated as shown in Fig. 7 (a). In comparison with Fig. 6, the spectrum exhibits completely different feature in which the two peaks (I^- and I^+) corresponding to the coupled intersubband plasmon-GaAs confined LO phonon modes dominate the spectra while other peaks due to IF modes diminish dramatically. This suggests the importance of the relative coupling-strengths among these modes, which affects strongly the effective interaction and results in the relative strength of Raman scattering cross-section. To demonstrate more clearly, in Figs. 7 (b) and (c) we show the calculated cross-sections for other two ACDQWs samples corresponding to two samples in Figs. 5 (b) and (c).

In Fig. 7 (a) the subband separation E_2-E_1 is chosen to be much less than energy of GaAs confined LO phonon (~36.25 meV) so that coupling between intersubband plasmon and this confined mode is dominant, and furthermore I^- peak is stronger than that of I^+. In Fig. 7 (b) the value of E_2-E_1 is selected between the energy of GaAs confined LO phonon and AlAs-like 2 IF phonon (~ 44.8 meV), and the coupling with GaAs confined LO phonon is still domonant, but intensity of I^+ peak becomes stronger than that of I^- peak. It is interesting to compare the related intensity of I^+ and I^- peaks in Figs. 7 (a) and (b). We can see that the peak intensity of I^+ in Fig. 7 (a) and I^- in Fig. 7 (b) are reduced very much compared with those of I^- and I^+ peaks in Fig. 7 (a) and in Fig. 7 (b), respectively. This indicates a characteristic feature of the ionic screening effect on the coupled modes strengths for the CDE scattering mechanism which was pointed out in our earlier study on the light scattering in single heterojunctions.[20] In Fig. 7 (c) when E_2-E_1 is closer to the energy of AlAs-like 1 IF phonon mode (~ 47.28 meV), coupling with this IF mode is dominant and it leads to the largest scattering cross-section near this IF mode energy.

Now we will discuss the lasing action in IRL by using rate eqs. (21a)–(21c). In Figs. 8 (a) and 8 (b) we show one typical result of temporal evolution of Stokes photons for I^- and I^+ modes and of population in subband 1 and 2 corresponding to lasing I^+ mode for the ACDQWs with E_2-E_1=36.92 meV (Fig. 7 (b)). The values of cross-sections, subband-electron relaxation times for the electron-optical and acoustic phonon scattering, cavity life-time of photon and the pumping intensity are listed in Table I. Figure 8 (a) shows that stimulated Stokes photon density related to I^+ mode extremely increased up to 10^{22} m^{-3} while that of I^- mode increased 10^6 within 200 ps. Therefore, we can expect the presence of I^+ mode in lasing. From Fig. 8 (b) it is evident that IRL operates in noninverted population scheme. Assuming an appropriate wave guiding structure for IRL[21], we have also predicted the temporal pulse profile of output power as depicted in Fig. 9. Taking the geometry of side-pumping with perpendicular polarization to the layer plane of

ACDQWs as in Fig. 2 (a), we can predict the transverse magnetic TM lasing-mode in consistent with the experiment.

We have also calculated the temporal variations of Stokes photons and subband populations for other two ACDQWs samples by applying eqs. (21a)–(21c). From these we can conclude that in the IRL only these coupled modes will induce the stimulated Stokes scattering, and then the lasing Stokes frequency is shifted from the pump frequency by the amount of one of these coupled modes frequencies. Therefore the selective occurrence of these coupled modes in lasing is governed by the electron-phonon coupling strengths which are predominantly determined by the subband separation (E_2-E_1) and the energies of confined LO and 6 IF phonon modes. These results are well consistent with the experiments[9] where the presence or lack of lasing related to the Raman Stokes shifts in some frequency ranges was found when several ACDQWs samples with different subband energy separations E_2-E_1 were used.

Finally, Fig. 10 shows the plot of calculated optimal Raman gain versus pump intensity. The calculated optimal detuning is δ_{opt} =7.04 meV and threshold intensity is I_{th} = 204 kW cm^{-2}. The dashed line shows the linear increase of gain with increasing pump intensity. However, taking into account the population N_2 the gain does not increase linearly and is saturated at high pumping intensities, as depicted by solid curve in the figure, which is in agreement with the experimental results.[9]

5. Concluding remarks

In the present paper, we have developed a microscopic gain theory for the intersubband unipolar Raman laser based on the stimulated electronic Raman scattering due to the collective excitations of coupled intersubband plasmon-phonon modes in asymmetric coupled double quantum wells structure (ACDQWs). Based on the charge-density-excitation mechanism, the

electron-electron and electron-optical phonon interactions including the confined-LO phonon and interface optical phonon modes are taken into account together with the self-consistent ACDQWs subband structures. Explicit derivation for the spectral differential scattering cross-section is given in terms of the dynamical response function χ using the Green's function method within the RPA framework. Stimulated Raman gain factor and self-consistent rate equations are then given in terms of the scattering cross-section. The optimization of Raman gain is given by changing a detuning factor, and the gain saturation at high pumping intensities is derived. Threshold gain and threshold intensity are also given. From the model calculations with three different ACDQWs structures we find that in IRL the lasing occurs at the Stokes frequencies shifted from pump frequencies by a constant value of one of the coupled intersubband plasmon-phonon modes, and our calculated results show that these coupled mode frequencies are determined by the coupling strength of electron-phonon interactions. In charge-density-excitation (CDE) mechanism we have emphasized the important role of ionic screening effect on the cross-section of intersubbnad plasmon-confined LO phonon modes. By adjusting the structural parameters of ACDQWs, it can be possible to make the lasing frequencies shifted from pump frequencies at the desired values.

In conclusion our theory not only can explain very well to understand the presence or lack of lasing modes for some frequency ranges of Raman shifts as observed in IRL experiments but also may provide a basis to design the more efficient IRL devices.

Acknowledgement

The authors would like to thank Dr. H. C. Liu for sending the pre-print papers and giving the valuable discussion about the experimental results at the National Research Council, Ottawa, Canada. This work was partly supported by a Grant-in Aid for the scientific Research Project from Ministry of Education, Culture, Sports, Science and Technology of Japan.

References

1) J. Faist, F. Capasso, D. L. Sivco, C. Sirtori, A. L. Hutchinson and A. Y. Cho: Science **264** (1994) 553.

2) J. Faist, F. Capasso, C. Sirtori, D. L. Sivco and A. Y. Cho: *Intersubband Transitions in Quantum Wells*: *Physics and Device Applications II*, Vol. 66 of *Semiconductors and Semimetals*, edited by H. C. Liu and F. Capasso (Academic, San Diego, 2000) Chap.1.

3) P. K. Basu: *Theory of Optical Processes in Semiconductors*: *Bulk and Microstructures* (Clarendon Press, Oxford, 1997) p. 191.

4) F. H. Julien, A. Sa'ar, J. Wang and J. P. Leburton: Electron. Lett. **31** (1995) 838.

5) Gauthier-Lafaye, P. Boucaud, F. H. Julien, S. Sauvage, S. Cabaret, J. M. Lourtioz, V. Thierry-Mieg and R. Planel: Appl. Phys. Lett. **71** (1997) 3619.

6) J. B. Khurgin, G. Sun, L. R. Frienman and R. A. Soref: J. Appl. Phys. **78** (1995) 7398.

7) H. C. Liu, I. W. Cheung, A. J. Spring Thorpe, C. Dharma-wardana, Z. R. Wasilewski, D. J. Lockwood and G. C. Aers: Appl. Phys. Lett. **78** (2001) 3580.

8) H. C. Liu, C. Y. Song, Z. R. Wasile wski, D. J. Lockwood, G. C. Aers, C. D. Wardana and A. J. SpringThorpe: Proc. of the 26th Int. Conf. on Physics of Semiconductors (Inst. of Phys. Pub. 2003) P134.

9) H. C. Liu, C. Y. Song, Z. R. Wasilewski, A. J. Spring Thorpe, J. C. Cao, C. Dharma-wardana, G. C. Aers, D. J. Lockwood and J. A. Gupta: Phys. Rev. Lett. **90** (2003) 077402.

10) G. S. He and S. H. Liu: Physics of nonlinear optics (World Scientific, 1999) p. 193.

11) G. D. Mahan: *Many-Particles Physics* (Kluwer, New York, 2000) p. 325.

12) M. Born and K. Haung: *Dynamical Theory of Crystal Lattices* (Clarendon, Oxford, 1968)

13) J. J. Licari and R. Evrard: Phys. Rev. B **15** (1977) 2254.

14) N. Mori and T. Ando: Phys. Rev. B **40** (1989) 6175.

15) R. Zheng and M. Matsuura: Phys. Rev. B **60** (1999) 4937.

16) S. G. Yu, K. W. Kim, M. A. Stroscio, G. J. Iafrate, J. P. Sun and G. I. Haddad: J. Appl. Phys. **82** (1997) 3363.

17) S. Katayama and T. Ando: J. Phys. Soc. Jpn. **54** (1985) 1615.

18) N. Bloembergen and Y. R. Shen: Phys. Rev. A **133** (1964) 37.

19) A. Yariv: *Quantum Electronics* (John Wiley & Sons, 1975) p. 168.

20) S. M. Maung and S. Katayama: *Proceedings of the 28th International Symposium on Compound Semiconductor*, Inst, Phys. Conf. Ser. No. **170** (2002) 443.

21) H. C. Liu and A. J. SpringThorpe: Phys. Rev. B **23** (2000) 15629.

Figure Captions

Fig. 1. Schematic view of a modulation-doped ACDQWs structure.

Fig. 2. (a) Geometry of pump and Stokes laser emission in ACDQWs based-IRL. The dashed region indicates the multiple quantum wells (MQW). (b) Schematic diagram of Raman scattering process through intersubband transitions.

Fig. 3. Calculated self-consistent conduction subband profile and electron wave functions in three subbands of ACDQWs with w_1=75 Å, w_2=60 Å, and $N_s = 3\times10^{11}$ cm^{-2} at T=80 K.

Fig. 4. Dispersion relations of the 12 IF phonon modes for a ACDQWs structure with w_1=75 Å, w_2=60 Å, b_1=200 Å and b_2=11.3 Å..

Fig. 5. Normalized electrostatic potentials of the 6 IF phonon modes at kb_1=0.016 in ACDQWs with corresponding structural parameters as shown in (a), (b) and (c).

Fig. 6. Calculated cross-section for a ACDQWs structure with w_1=75 Å, w_2=60 Å assuming the same value of coupling constant with electron for all optical phonon modes.

Fig. 7. Calculated cross-sections versus Raman Stokes shift in cases of (a) E_2-E_1< $\hbar\omega_{LO}$ (GaAs confined-LO), (b) $\hbar\omega_{LO} < E_2$-$E_1 < \hbar\omega_{IF2}$ (AlAs-like 2 IF phonon) (c) E_2-E_1~ $\hbar\omega_{IF1}$ (AlAs-like 1 IF phonon) for three ACDQWs structures with different structural parameters shown in the figures.

Fig. 8. (a) Time evolution of stimulated Stokes photon densities due to lasing by Γ^+ and Γ^- coupled modes, (b) temporal variation of populations in subband 1 and 2 for lasing Γ^+ mode.

Fig. 9. Time evolution of output power profile in the ACDQWs laser device.

Fig.10. The IRL gain spectra (solid line) as a function of the pumping intensity for the optimal detuning δ_{opt}=7.04 meV. The dashed curve shows the saturated Raman gain at high-intensity pumping levels.

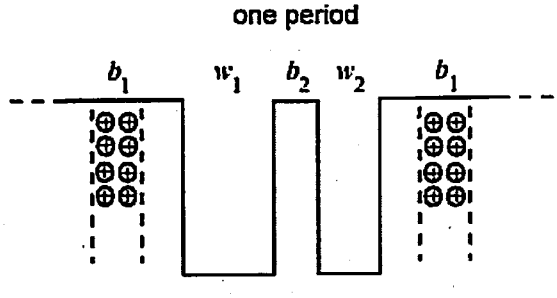

Fig. 1

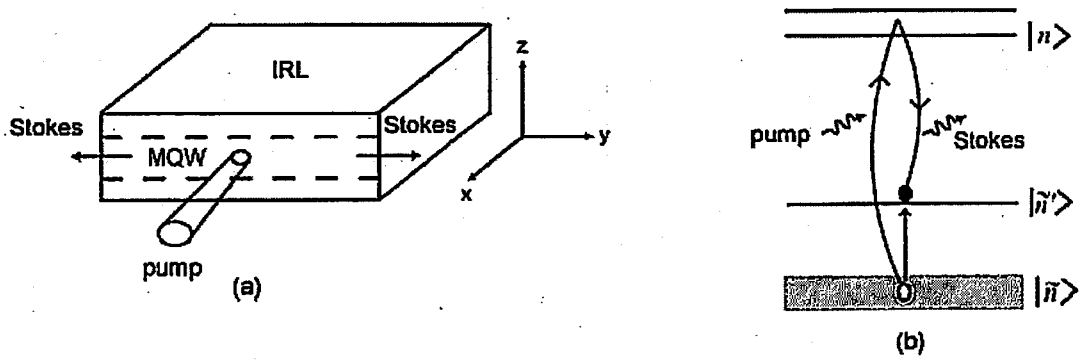

Fig. 2

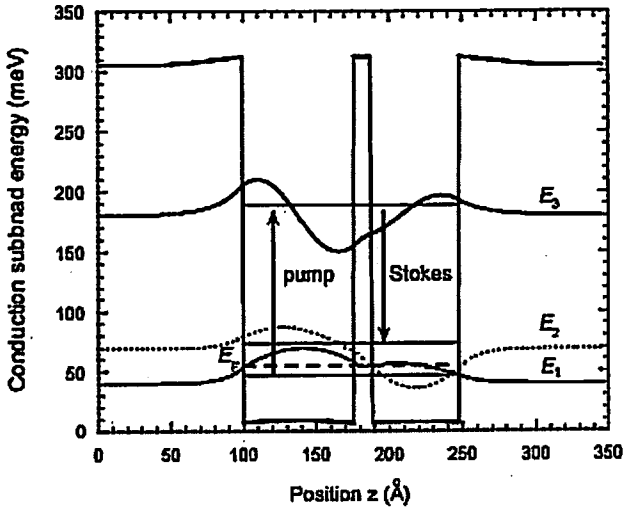
Conduction subbnad energy (meV)
Position z (Å)
pump
Stokes
E3
E2
E1
E0
0
50
100
150
200
250
300
350

Fig. 3

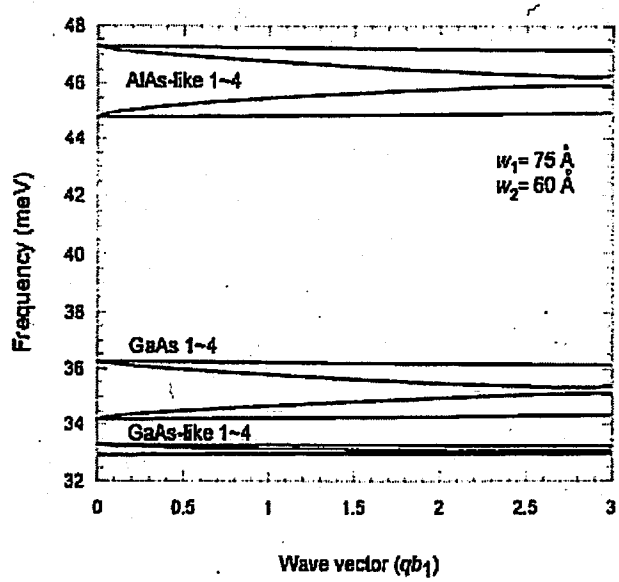
48
46
44
42
40
38
36
34
32
AlAs-like 1~4
w_1= 75 Å
w_2= 60 Å
GaAs 1~4
GaAs-like 1~4
Frequency (meV)
0
0.5
1
1.5
2
2.5
3
Wave vector (qb_1)

Fig. 4

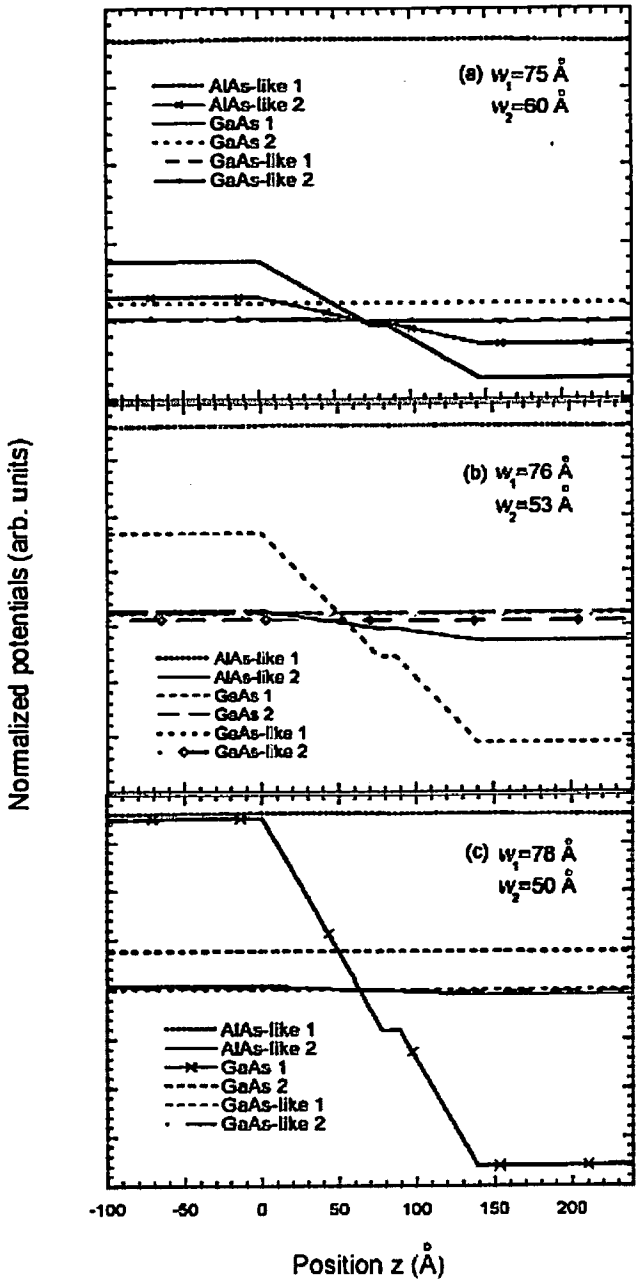
(a) w_1=75 Å
w_2=60 Å
AlAs-like 1
AlAs-like 2
GaAs 1
GaAs 2
GaAs-like 1
GaAs-like 2
(b) w_1=76 Å
w_2=53 Å
AlAs-like 1
AlAs-like 2
GaAs 1
GaAs 2
GaAs-like 1
GaAs-like 2
(c) w_1=78 Å
w_2=50 Å
AlAs-like 1
AlAs-like 2
GaAs 1
GaAs 2
GaAs-like 1
GaAs-like 2
Normalized potentials (arb. units)
-100
-50
0
50
100
150
200
Position z (Å)

Fig. 5

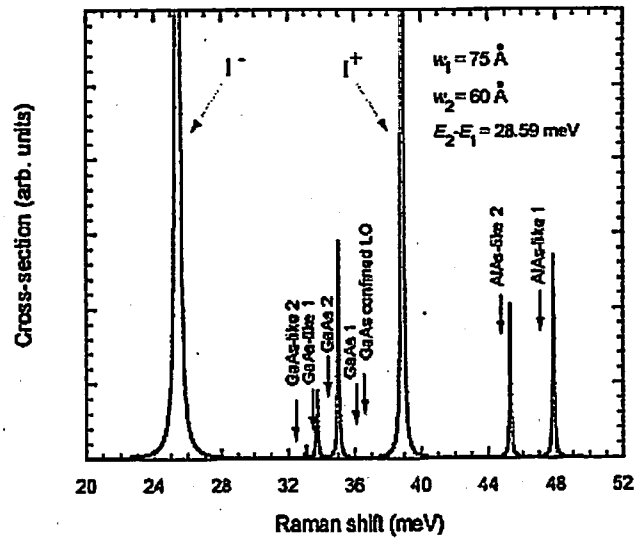
I⁻
I⁺
w₁ = 75 Å
w₂ = 60 Å
E₂-E₁ = 28.59 meV
GaAs-like 2
GaAs-like 1
GaAs 2
GaAs 1
GaAs confined LO
AlAs-like 2
AlAs-like 1
Cross-section (arb. units)
20
24
28
32
36
40
44
48
52
Raman shift (meV)

Fig. 6

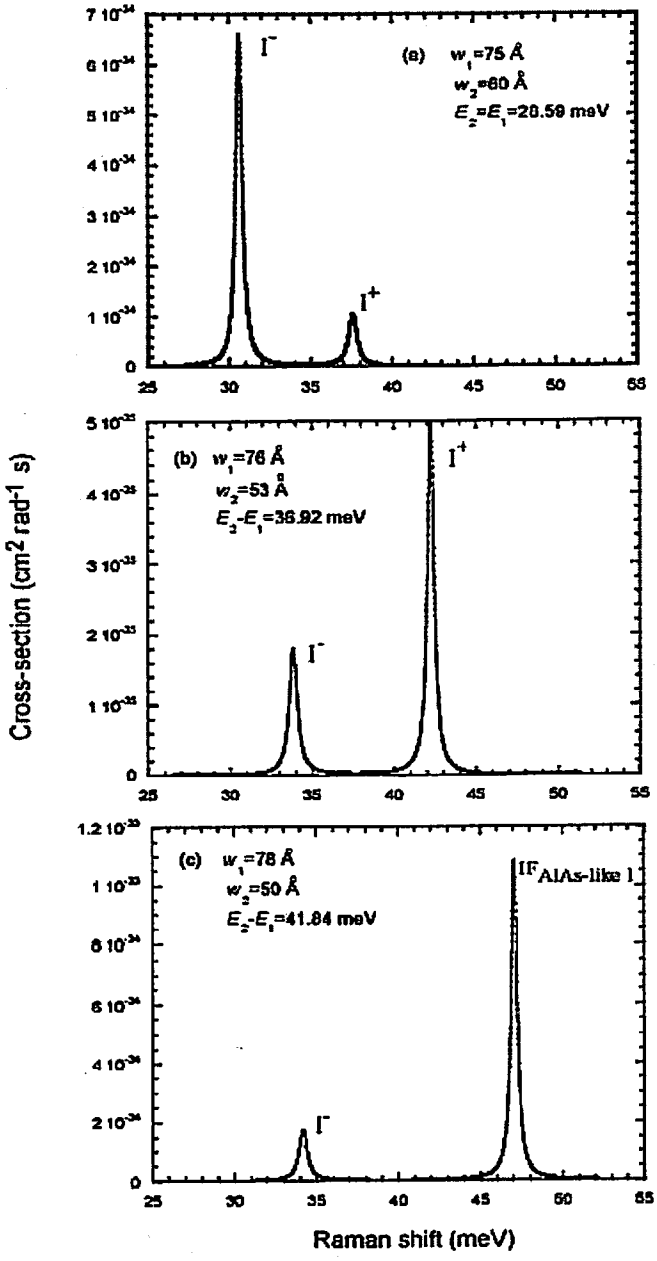
(a) w1=75 Å
w2=60 Å
E2-E1=28.59 meV
I-
I+
(b) w1=76 Å
w2=53 Å
E2-E1=38.92 meV
I+
I-
(c) w1=78 Å
w2=50 Å
E2-E1=41.84 meV
IF AlAs-like 1
I-
Cross-section (cm2 rad-1 s)
Raman shift (meV)

Fig. 7

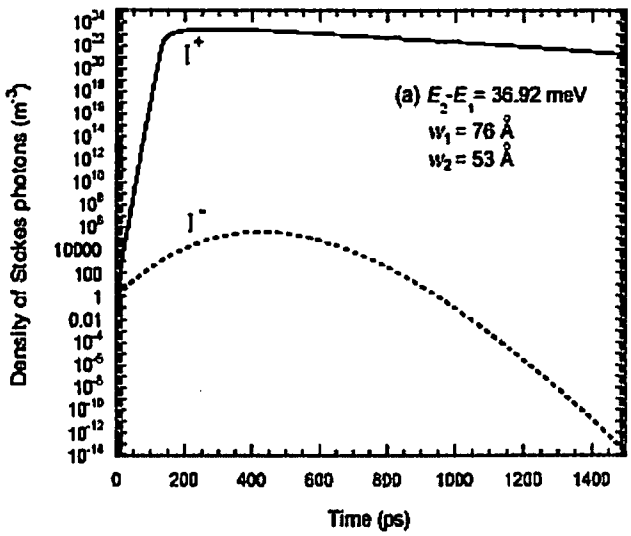
Density of Stokes photons (m^{-3})
I^+
I^-
(a) E_2-E_1 = 36.92 meV
w_1 = 76 Å
w_2 = 53 Å
Time (ps)

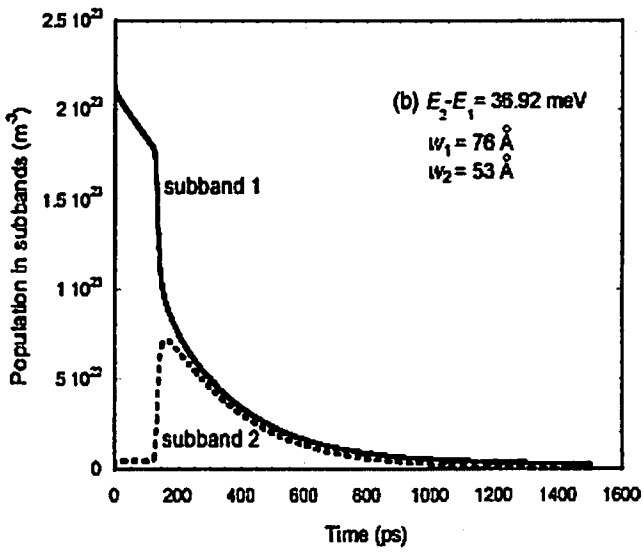
Population in subbands (m^{-3})
subband 1
subband 2
(b) E_2-E_1 = 36.92 meV
w_1 = 76 Å
w_2 = 53 Å
Time (ps)

Fig. 8

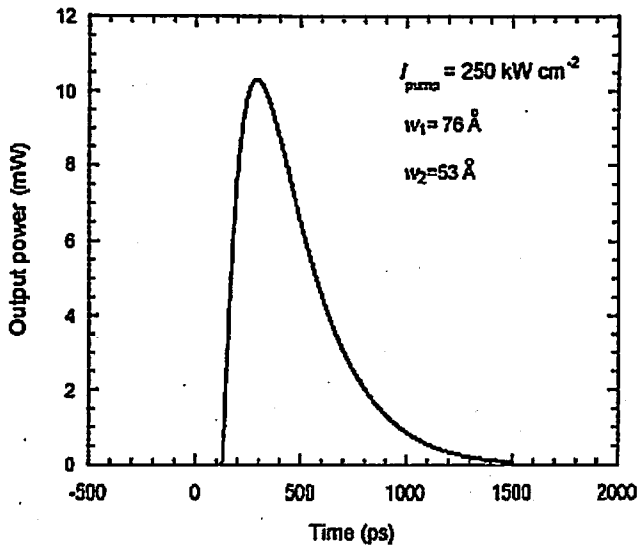
12
10
8
6
4
2
0
-500
0
500
1000
1500
2000
Output power (mW)
Time (ps)
I_{pump} = 250 kW cm^{-2}
w_1= 76 Å
w_2=53 Å

Fig. 9

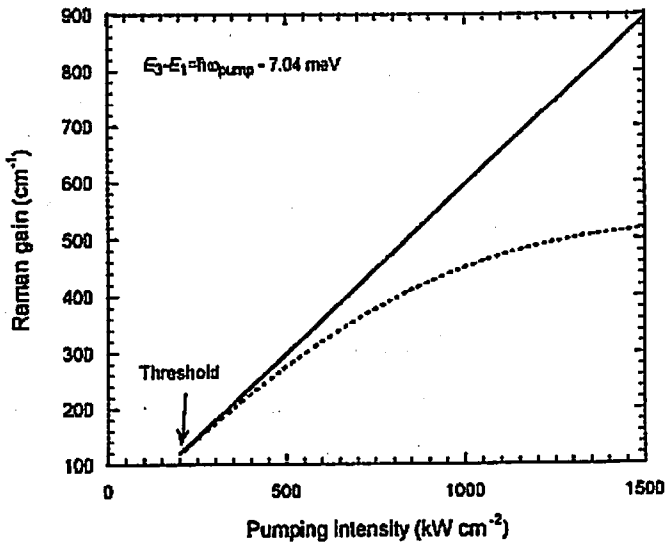
900
800
700
600
500
400
300
200
100
0
500
1000
1500
Raman gain (cm^{-1})
Pumping intensity (kW cm^{-2})
E_3-E_1=$\hbar\omega_{pump}$ = 7.04 meV
Threshold

Fig. 10

Table I. Numerical values used in the rate equations.

Parameter	unit	value
Spectral differential scattering cross-section	$\frac{d^2\sigma}{d\omega d\Omega}$ ($cm^2\,sr^{-1}\,s$)	0.181×10^{-34} (I^-) 0.496×10^{-34} (I^*)
2 to 1 relaxation time	τ_{12} (s)	0.2265×10^{-12}
1 to 2 relaxation time	τ_{21} (s)	0.1011×10^{-10}
Photon cavity life-time	τ_c (s)	9.576×10^{-11}
Effective relaxation time of subband 1	τ_1^{eff} (s)	0.9029×10^{-12}
Effective relaxation time of subband 2	τ_2^{eff} (s)	0.223×10^{-12}
Pumping laser intensity	I_{pump} ($kW\,cm^{-2}$)	250